LANGMUIR



Article

# Dip-and-Drag Lateral Force Spectroscopy for Measuring Adhesive Forces between Nano-fibers

Grace Kathryn Dolan, Gleb E. Yakubov, George W. Greene, Nasim Amiralian, Pratheep Kumar Annamalai, Darren J. Martin, and Jason R Stokes

*Langmuir*, **Just Accepted Manuscript** • DOI: 10.1021/acs.langmuir.6b03467 • Publication Date (Web): 22 Nov 2016

# Dip-and-Drag Lateral Force Spectroscopy for Measuring Adhesive Forces between Nano-fibers

Grace K. Dolan[a,b], Gleb E. Yakubov[a,b,*], George W. Greene[c], Nasim Amiralian[d], Pratheep K. Annamalai[d], Darren J. Martin[d], Jason R. Stokes[a,b]

[a] School of Chemical Engineering, The University of Queensland, Brisbane 4072, Australia

[b] Australian Research Council Centre of Excellence in Plant Cell Walls, The University of Queensland, Brisbane 4072, Australia

[c] The Institute for Frontier Materials and The Australian Center for Excellence in Electromaterials Science, Deakin University, Waurn Ponds, VIC 3216 Australia

[d] Australian Institute for Bioengineering and Nanotechnology (AIBN), The University of Queensland, Brisbane 4072, QLD, Australia

Adhesive interactions between nano-fibers strongly influence the mechanical behavior of soft materials comprised of fibrous networks. We use atomic force microscopy (AFM) in lateral force mode to drag a cantilever tip through fibrous networks, and use the measured lateral force response to determine the adhesive forces between fibers of the order of 100 nm diameter. The peaks in lateral force curves are directly related to the detachment energy between two fibers; the data is analyzed using the Jarzynski equality to yield the average adhesion energy of the weakest links. The method is successfully used to measure adhesion forces arising from van der Waals interactions between electrospun polymer fibers in networks of varying density. This approach overcomes the need to isolate and handle individual fibers, and can be readily employed in the design and evaluation of advanced materials and biomaterials which, through inspiration from nature, are increasingly incorporating nano-fibers. The data obtained with this technique may also be of critical importance in the development of network models capable of predicting the mechanics of fibrous materials.

## INTRODUCTION

Inter-fiber adhesion is a key factor in the functionality of naturally occurring fibrous assemblies such as collagen,[1] cellulose assemblies from plant material,[2,3] and recently emerging synthetic advanced biomaterials.[4,5] The ubiquity of fibrous structures in nature calls for the development of techniques enabling the direct measurements of adhesion between nanofibers. These techniques are set to play an important role in biomimetic design since fiber-fiber interactions are of fundamental importance to the overall network mechanics and material performance. This has been demonstrated in tissue engineering; for example, graft materials are designed to mimic the fibrous structure of extracellular matrices to optimize their mechanical properties so as to promote cell adhesion and migration.[6,7]

The mechanical properties of a range of fibrous materials have been studied using compression, uni- and bi-axial tensile testing and small-amplitude oscillatory shear.[8-18] The results from these studies indicate that the mechanics of random fiber networks is defined by the intrinsic mechanical properties of nanofibers, surface interactions between fibers, the network microstructure, and number and nature of entanglements and/or cross-links, as well as the solvent properties that affect the Hamaker constant and thus the adhesive interactions between fibers.

The development of structural models of fiber networks provides predictive capabilities for design and evaluation, as well as enhancing understanding of the underlying principles controlling natural systems. The common approach to account for the adhesive potential is to simply treat contacts between fibers as rigid junctions,[19-22] which is only appropriate when fiber interactions are very strong. For viscoelastic fiber networks, Chatterjee[23] applied an energy penalty to the breaking of each fiber-fiber contact and related it to the stored elastic energy of deformation.[23] However, a reliable model for any particular system requires accurate knowledge of the adhesive potential between fibers at network junctions, which is only obtained through experiments.

Direct measurement of fiber adhesion has been achieved for sub-micron (>100 nm) electrospun fibers through a variety of elaborate experiments. These include fixing freestanding fibers by taping them to cardboard mounts,[24,25] or gluing them between two microspheres on an AFM cantilever.[26] In these systems, two fixed fibers are arranged orthogonal to each other at the midpoint in a cross-cylinder configuration and pressed into contact for a given time. The applied load and vertical displacement

are monitored as the fibers are pulled apart at a constant speed and the pull-off force is measured. Shi et al.[24,25] show that for polycaprolactone and Nylon 6 fibers, the pull-off force increases linearly with radius of the fiber.[24,25] Stachewicz, et al.[27] take individual fibers and fix one end to a cantilever, then bring the free ends of two fibers together in a parallel orientation; the pull-off force is measured as the fibers are separated. The measured pull-off force critically depends on the fiber orientation because of its effect on contact area. It is challenging to use these methods to assess all the possible fiber orientations between parallel and orthogonal, that are observed in randomly assembled fibrous networks. Another limitation of these techniques is the inability to measure the potential for fibers to interact via mechanical entanglement whereby fibers wrap around each other. Xing, et al.[28] show that there is a significant effect on adhesion if fibers are permitted to wrap around each other. In their experiment an electrospun polystyrene nanofiber is observed to wrap around a nanoparticle attached to an AFM tip. Despite recent progress in measuring forces between fibers, for the absolute majority of fibrous systems it is difficult to extract individual fibers. Additionally, direct handling of nano-fibers with thicknesses below 100 nm is prohibitive.

In this paper, we provide a novel approach using lateral force microscopy on an AFM to measure the adhesive-detachment forces between fibers *in situ*, that is, within the fiber network. We refer to this as a 'dip-and-drag' technique, as it involves inserting an AFM tip into the network and dragging it laterally. We show how peak forces are related to detachment events between fibers as they are pulled apart from each other by the cantilever, and we validate the method using well-characterized electrospun polymer fibers fabricated from sulfonated polyether ether ketone (SPEEK) and polyvinyl alcohol (PVA). In these systems the adhesive forces are dominated by DLVO interactions, making them suitable for testing the novel technique.

## MATERIALS AND METHODS

**Electrospun sulphonated polyether ether ketone (SPEEK) fibers.** SPEEK with a 75% degree of sulphonation, as determined by $H^1$ NMR, was prepared from Victrex polyether ether ketone 450PF (PEEK; $M_w$ = 38,300) following the protocols outlined by Huang, et al.[29] A solution of PEEK was prepared in concentrated sulfuric acid (95-97%) at room temperature under mechanical stirring at a concentration ratio of 5/95 (w/v). Once complete dissolution of the PEEK was achieved, the solution was sealed in a solution bottle and incubated in an oven at 36ºC for 15 hours. The SPEEK was then precipitated from solution by the addition of deionized water from a MilliQ Advantage A10 system with resistance 18 Ω.cm at 25°C. The precipitated SPEEK powder was recovered using filtration and washed thoroughly with clean deionized water to remove any residual acid. The recovered and washed SPEEK powder was then dried in a vacuum oven at 50ºC for approximately 48 hours to remove any residual water.

For electrospinning, a solution of 15% wt SPEEK was prepared in dimethylformamide on a hotplate at 60°C under mechanical stirring for 24 h. The SPEEK solution was loaded into a 1 ml Hamilton syringe which was fixed with a blunted 20G x 1½ in. stainless steel syringe needle. The syringe was loaded onto a syringe pump and the syringe needle was connected to a high voltage power supply (Gamma High Voltage Research, USA). A clean glass microscope slide was mounted to a grounded collection plate using double sided tape and the collection plate and slide were covered with aluminum foil. A hole was cut out of the center of the aluminum foil to expose an approximately 1 cm x 1 cm area of the underlying glass slide. The collection plate was then positioned 17 cm away from the tip of the syringe needle. The electrospinning was done by pumping the SPEEK solution through the syringe under a constant flow rate of 0.12 ml/hr under an applied voltage of 20 kV to the syringe needle. The SPEEK nanofibers were electrospun onto the substrate for a given time ranging from 1 to 5 minutes, resulting in fiber matts with varying network densities. The SPEEK nanofiber network was then imaged using a NeoScope JCM-5000 Scanning Electron Microscope (SEM) (JEOL) and the average fiber diameter, 127±9.3 nm, was obtained directly from the SEM micrographs and analyzed using ImageJ software (Figure 1a).

**Electrospun Polyvinyl Alcohol (PVA) fibers.** PVA polymer (molecular weight of 85-124 kg/mol -Sigma-Aldrich, Castle Hill, Australia) was firstly dissolved in deionized water at 80°C for four hours, the solution was left to stand, unstirred, for a few minutes in order to degas before electrospinning. For the electrospinning process, polymer solution was loaded into a 5 ml syringe and a positive electrode was clipped onto the syringe needle with a 0.5 mm diameter. The flow rate of the PVA solution was 0.5 mm/hour, at an applied voltage of 22 kV and tip to collector distance of 13 cm. PVA solution was electrospun horizontally onto the target. After electrospinning, the collected nanofiber mat was dried in vacuum oven at 60°C for 8 hours. The morphology of PVA nanofibers was investigated using a JSM-6460LA SEM (JEOL). From the SEM images the average diameter of 50 individual nanofibers obtained was 163 ± 42 nm (Figure 1b).

**Lateral Mode Force Spectroscopy using manipulation control.** SPEEK fibers were electrospun directly onto a glass slide. For PVA, small sections (ca. 5mm x 5mm) of network are adhered to a glass slide, leaving one edge exposed, using 5-minute curing epoxy resin (UHU GmbH & Co. KG, Germany) (equal parts base and curing agent).

The JPK Nanowizard II AFM was mounted on an inverted optical microscope (JPK Instruments, Germany). The AFM was loaded with a stiff cantilever (HQ:NSC35/Cr-Au BS, Cantilever A) from Mikromasch

(Nano World AG, Germany). The networks were first imaged in intermittent contact mode in air to identify the exposed edge. The imaging is performed at a scan rate of 2 Hz for a 60 x 60 μm scan size with 1024 x 1024 pixels. The set point and drive amplitudes are around 1 V and the drive frequency is around 200 kHz. Using manipulation control in contact mode, a cantilever path was traced over the image such that the tip was engaged around the exposed edge of the network for PVA, or anywhere inside the homogeneous network for SPEEK samples, and then dragged outward to measure fiber detachment events as illustrated in Figure 2. For lateral force measurements the set point vertical deflection was 300 nN and the cantilever travel speed was 0.3 μm/s. This lateral force measurement was repeated several times on different parts of the network. The initial placement of the AFM tip inside the network is random and in some cases may land on a fiber rather than the substrate. Force-distance curves with an initial constant baseline force, where the lateral force is equal to the substrate friction as depicted in Figure 2, are selected for analysis to ensure that a set point vertical force is established between the AFM tip and the substrate. The test was repeated for a given SPEEK fiber sample with aniline (Sigma) as a solvent. Aniline has a refractive index between that of glass and SPEEK causing negative van der Waals interactions that substantially reduce the adhesion between the fibers and substrate.[30] By contrast, aniline has only a marginal effect on adhesive forces between SPEEK fibers, because van der Waals interaction between surfaces of the same material is always attractive.[31] Subsequently, the results are compared to those obtained from the measurement in air to confirm that the recorded forces are due to fiber-fiber interactions and not influenced by fiber-substrate adhesion.

The lateral deflection data was recorded during the cantilever trace and converted to lateral force. The Torsional Sader Method[32] was used to find the torsional spring constant, and the lateral sensitivity was calculated using a non-contact calibration procedure.[33]

## RESULTS AND DISCUSSION

**Dip-and-Drag Lateral Force Spectroscopy of SPEEK electrospun mats of varying network density.** Figure 3 presents lateral force-distance measurements obtained for SPEEK fiber samples at two extremes of network density. The AFM tip is engaged with the substrate and translated laterally whilst maintaining a constant normal force. During dragging, the baseline force is due to a combination of friction between the tip and substrate, and elastic deformation of the network. For low network density, we suggest that the fibers are sufficiently far apart that a single fiber is pulled without deforming large sections of the network. Thus the relatively constant baseline force (designated 'bf') in Figure 3a is anticipated to be dominated by tip-substrate friction. In contrast, the lateral force measured for the dense fiber network in Figure 3b is steadily increasing, suggesting a baseline force that is dependent on degree of network deformation. The baseline force in Figure 3b is initially constant, confirming that the AFM tip first comes into contact with the substrate at the set point vertical force before contacting fibers with lateral movement. We suggest that the overall increase in lateral force corresponds to the AFM tip dragging a number of fibers collectively, which leads to a large and cumulative contribution of network deformation to the measured force.

In the force-distance profiles of SPEEK samples with low network density, we observe consistent peaks above the baseline force (designated by * in Figure 3a). We propose that the observed sharp increase in lateral force (above the baseline) corresponds to the cantilever tip engaging with a fiber and bringing it into tension. The abrupt decrease in lateral force is proposed to be associated with a detachment event at a fiber-fiber contact, such that the fiber is no longer in tension and the signal returns back to the baseline value. Figure 3a indicates where we take the height of the peak force (designated by 'h') to be a measure of the force required for detachment at a fiber contact, which is akin to a 'pull-off' force between fibers. Figure 4a is an SEM image of the SPEEK fiber substrate superimposed with a white line to represent a potential 2 micron length pathway for the lateral movement of the AFM covered in Figure 3a. Whilst this particular image does not necessarily correspond to the section of the fiber network that is measured, it provides an indication that the fiber detachment events occur in line with the density of fiber interactions (designated by * in Figures 3a and 4a). The image shows that it is plausible that 4 contacts are probed during measurement over the 2μm lateral distance whilst maintaining a stable baseline force.

For high network density samples, a sharp drop in the lateral force is observed relative to the deformation-dependent baseline force (Figure 3b). In this case, the measured force is expected to be distributed across a number of fiber contact points. We suggest that when the local force at a single contact point exceeds the adhesion force, fiber-fiber detachment occurs, seen as a sharp drop in the measured lateral force. The peak height or pull-off force is labelled 'h' in Figure 3b. In Figure 4b a 7μm trace is marked that corresponds to 7 fiber contacts being disrupted. The fibers that are pulled during the trace have remaining connections to the network leading to large scale deformation and an increasing baseline force. This proposed trace is consistent with the observations in Figure 3b.

In Figure 3 there is an initial decrease in the z-piezo position of the cantilever (right axis in Figure 3a and 3b) which corresponds to an overshoot of the vertical deflection before settling to the set point with changing height. The overall drift in the height, particularly in Figure 3b, is attributed to optical crosstalk between the photodetector signals related to normal and torsional deflections of the cantilever. Due to rotational misalignment of the photodetector during lateral force

measurements, the vector representing the lateral shift of the laser has a non-zero vertical shift.[34] A substantial height change is observed in Figure 3b at a distance of around 6.5μm, which we suggest is due to fiber breakage. The frequency of these types of events can be determined by histogram analysis of the population of peak heights.

The entire set of force-displacement curves are analyzed using a semi-automated MATLAB routine. The code identifies a peak if the average force of *x* number of consecutive points on either side is less than the force at the point of interest. The value of *x* is adjusted for the background noise frequency. The local maximum and minimum of the identified peaks are found. The peak height is taken as the distance between the maximum and subsequent minimum.

Figure 5a shows a representative force-distance curve for the lowest network density SPEEK sample with the baseline force subtracted. The peak heights extracted from the set of fiber pulling measurements are presented in a histogram in Figure 5b. The tail of the distribution at large peak heights is attributed to the situations where the cantilever cuts through the fibers or, which are shown to occur with low frequency.

Peak heights correspond to fiber detachment events when a fiber under tension is released from the network either by the fiber breaking or the adhesion between fibers at a contact zone being overcome. SEM images of the different SPEEK samples after testing, labelled A through to E, are shown in Figure 6. There is evidence of broken fibers, however some broken fibers are also observed for SPEEK samples that have not been measured using the dip-and-drag technique. Furthermore, the broken fibers seem to largely occur around the globular structures, as seen in Figure 6, and could be an artefact of the electrospinning process. We cannot rule out that some fiber breakage may be occurring but the overall increasing baseline force in Figure 3b suggests that fibers remain in tension. We compare experimental results to theoretical adhesion energies in the next section to support our interpretation of the peak heights as a measure of the adhesion between fibers.

The shape of the distribution is largely influenced by the fiber network density and the number of contacts that are in tension just prior to a detachment event occurring. To illustrate this point, two scenarios of dragging a fiber are considered. As depicted in Figure 7a, either the pulling force is applied at a single fiber contact or divided between two fiber contacts. For the first scenario, the pulling force ($F_{\mathrm{TOTAL}}$) is equal to the adhesion force ($F_{\mathrm{adh}}$) at the single contact zone. For the second scenario the cantilever tip can pull from any point along a fiber connecting two contact zones where the two distances are labelled $L_1$ and $L_2$. The pulling force stretches the fiber by the distance 2δ, and hence the strain applied to each segment of the fiber is ~$\delta/L_1$ and ~$\delta/L_2$. The detachment at the weakest contact zone, either **1** or **2**, occurs when the resulting elastic force applied to the respective segment is equal to the adhesive force.

$$F_i = \pi R^2 E \frac{\delta_i^*}{L_i} = F_{\mathrm{adh}_i} \quad (1)$$

*R* is fiber radius, *E* is Young's modulus. Consequently, the strain at the pull-off is

$$\delta_i^* = \frac{L_i}{\pi r^2 E} F_{\mathrm{adh}_i} \quad (2)$$

Here we assume that the stretching force remains linear with deformation, and the pull-off force is independent of elastic parameters of the fiber. The resulting force is the sum of the forces applied to both segments of the fiber and is a function of the ratio of $L_1$ and $L_2$. We can write the expression for the total force using the Heaviside function as a convenient operator which 'selects' whether the detachment occurs at the contact **1** or the contact **2**. It can be seen from eq 3, that the total pulling force at the point of detachment is independent of elastic parameters of the fiber and depends only on the ratio of fiber segment lengths, $l = \frac{L_1}{L_2}$, and the force of adhesion $\left(F_{\mathrm{adh}_i}\right)$.

$$\mathrm{F_{TOTAL}} = F_1 + F_2 = \quad (3)$$
$$= \left[H(\delta_2^* - \delta_1^*) \cdot F_{\mathrm{adh}_1} l + H(\delta_1^* - \delta_2^*) \cdot F_{\mathrm{adh}_2}\right] \cdot \frac{1+l}{l}$$

*H()* is the Heaviside function. Each detachment event depends on the three random variables that contribute to the value of the force, $F_{\mathrm{adh1}}$ , $F_{\mathrm{adh2}}$ , and *l*. If $F_{\mathrm{adh1}}$ and $F_{\mathrm{adh2}}$ are assumed to be part of the same distribution $\{F_{\mathrm{adh}}\}$ then:

$$F_{\mathrm{TOTAL}} = \{F_{\mathrm{adh}}\} \cdot (1+l) \cdot \begin{cases} \frac{1}{l}, & l > 1 \\ 1, & l \le 1 \end{cases} \quad (4)$$

Further, if a uniform distribution of the random variable *l* is assumed, then the ensemble average force can be calculated as:

$$\langle F_{\mathrm{TOTAL}} \rangle = \frac{1}{l} \int_0^l F_{\mathrm{TOTAL}} dl \approx 1.2773 \cdot \{F_{\mathrm{adh}}\} \quad (5)$$

Therefore for the contact where the pulling force is divided between two fibers the measured force is expected to have a similar distribution to the adhesive force of a single junction with a correction coefficient of ~1.3, as shown in Figure 7b. Amongst many peak force distributions recorded, we have noticed that all feature a wide distribution of forces similar to the example shown in Figure 5b. Due to the breadth of the distributions, both scenarios are captured within the range of the most frequent event. Further refinement can be achieved by applying Jarzynski's averaging[35,36] to the data according to eq 6. This exponential averaging gives more weight to more frequent events that occur at low peak height values.

$$exp[-\Delta Q] = \lim_{n \to \infty} \langle exp[-h_i] \rangle_N \quad (6)$$

*Q* is the exponentially averaged peak height, $<>_N$ denotes arithmetic averaging of N peak events, and $h_i$ represents the peak height of the *i*th event.

Remarkably, the average peak heights for SPEEK samples show no dependence on the network density. The absence of a trend is apparent when comparing the

SEM images in Figure 6 with peak heights in Table 1; in particular samples D and E show the lowest fiber network density but not necessarily the lowest peak height. This provides evidence that regardless of whether the baseline force is deformation-dependent or not, the origin of the sharp-decrease or peak in lateral force is the same and likely to be a fiber-fiber detachment event. This supports the peak height representing a 'pull-off' force between two fibers in contact. Elastic deformation of the fiber network thus has little influence on the pull-off force, and the average for all samples is 8.4±1.4μN.

To confirm that the measured detachment events are not due to fiber-substrate interactions, the dip-and-drag technique is used to measure the forces for one of the SPEEK samples (E) with aniline as a solvent. Aniline has a refractive index between glass and SPEEK giving rise to repulsive van der Waals interactions between the fiber and substrate whilst maintaining attractive van der Waals interactions between fibers. There was found to be no statistically significant difference between the population of peak heights measured in air and aniline with a p-value of 0.96. Thus the detachment events measured are attributed to the interactions between fibers.

**Dip-and-Drag Lateral Force Spectroscopy of PVA network.** The present technique is further tested on a network of electrospun PVA fibers with an average diameter of 163 ± 42 nm. The force-distance curves for the PVA sample, an example of which is in Figure 8a, shows a large contribution of network deformation to the baseline force that is consistent with a highly dense network. The histogram of peak heights in Figure 8b is characterized by the exponentially averaged peak height of 6.1μN which we consider to be the PVA pull-off force for further analysis.

**Analysis of adhesive forces between fibers.** For the presented technique the subject fibers are not deliberately brought into compressive contact with a known load. It is therefore appropriate to consider electrospun polymer fibers in the network to be interacting through van der Waals forces. The electrospinning procedure gives reasonably cylindrical fibers and capillary forces are expected to be negligible for the contact angles created by two cylinders. We examine whether the order of magnitude of the measured pull-off forces for SPEEK and PVA fibers is comparable to the interaction forces ($F_{\mathrm{vdW}}$) predicted from van der Waals interaction energy between two cylindrical bodies in parallel configuration according to eq 7.[37] Parallel configuration allows us to specify the length ($L$) of fiber-fiber contact. We calculate $L$ for two fibers interacting with an orientation at the midpoint between parallel and orthogonal, that is, a 45° angle between longitudinal axes of fibers.

$$F_{\mathrm{vdW}} = \frac{\boldsymbol{A}_{\mathbf{H}} L\sqrt{R}}{16D^{5/2}} \qquad (7)$$

$\boldsymbol{A}_{\mathbf{H}}$ is the Hamaker constant, $R$ is the fiber radius and $D$ is the separation distance which is reported to be of the order of 1 Å for strong van der Waals interaction.[37] The comparison between theoretically calculated Hamaker constants and those predicted from the experiment are summarized in Table 2. The experimental values of the Hamaker constant are calculated using eq 7 and the values of the pull-off force 8.4 μN and 6.1 μN for SPEEK and PVA, respectively. Additionally, to test the effect of the pulling configuration on the measured force, the experimental pull-off forces are adjusted by applying the factor 1.3 in accordance with eq 5. The Hamaker constants computed this way correspond to the scenario where the dragging force is predominantly divided between two fiber contacts.

The predicted Hamaker constants are calculated using two methods. Firstly, we employ a method based on extracting the surface energies from the wetting data, which gives $A_{\mathrm{H_{SE}}}$ = 5.81 x10$^{-20}$ J and 10.5 x10$^{-20}$ J for SPEEK and PVA, respectively.[38,39] Secondly, we perform a full calculation based on the Lifshitz' theory of van der Waals forces[31], which gives $A_{\mathrm{H_L}}$ = 12.9 x10$^{-20}$ J and 10.5 x10$^{-20}$ J for SPEEK and PVA, respectively. In these calculations we use the integrated form of the equation for the free energy of interaction developed by Parsegian and Ninham.[40] The permittivity spectra were calculated using the method of Hough and White[41] based on the representation of the material's dielectric response $\varepsilon(i\xi)$ at the imaginary frequency ($i\xi$) as a sum of two damped Lorentz oscillators.[42]

$$\varepsilon(i\xi) = 1 + \frac{C_{\mathrm{UV}}}{\left(1 + \left(\xi/\omega_{\mathrm{UV}}\right)\right)} + \frac{C_{\mathrm{IR}}}{\left(1 + \left(\xi/\omega_{\mathrm{IR}}\right)\right)} \qquad (8)$$

All constants, $C_{\mathrm{UV}}$, $\omega_{\mathrm{UV}}$, $C_{\mathrm{IR}}$, $\omega_{\mathrm{IR}}$, are determined from the experimental data available in the literature. The $C_{\mathrm{UV}}$ and $\omega_{\mathrm{UV}}$ values are determined from the Cauchy equation and the refractive index spectra available for SPEEK[43] ($C_{\mathrm{UV}}$ = 1.6, $\omega_{\mathrm{UV}}$ =1.24×10$^{16}$ rad/s) and PVA[44] ($C_{\mathrm{UV}}$ = 1.5, $\omega_{\mathrm{UV}}$ =1.36×10$^{16}$ rad/s).

$$n^2(\omega) - 1 = C_{\mathrm{UV}} + (n^2(\omega) - 1)\frac{\omega^2}{\omega_{\mathrm{UV}}^2} \qquad (9)$$

The $\omega_{\mathrm{IR}}$ frequencies are evaluated based on FTIR spectra for SPEEK[45] and PVA.[44] The maximum absorption in the IR are found at 3451 cm$^{-1}$ ($\omega_{\mathrm{IR}}$ = 6.50×10$^{14}$ rad/s) and 2044 cm$^{-1}$ ($\omega_{\mathrm{IR}}$ = 3.85×10$^{14}$ rad/s) for SPEEK and PVA, respectively. The CIR is determined based on the approximate equation.[42]

$$C_{\mathrm{IR}} = \varepsilon_0 - C_{\mathrm{UV}} - 1 \qquad (10)$$

$\varepsilon_o$ is the static dielectric constant, which was determined from the electrical impedance measurements for SPEEK ($\varepsilon_o$ = 5, $C_{\mathrm{IR}}$ = 2.4)[46] and PVA[47] ($\varepsilon_o$ = 3, $C_{\mathrm{IR}}$ = 0.5).

The $\boldsymbol{A}_{\mathbf{H}}$ values for PVA calculated using wetting data and the Lifshitz' theory show an excellent agreement, and highlight the fundamental equivalency of both approaches. For SPEEK, the discrepancy is somewhat larger, which may be associated with changes in the SPEEK material in the presence of water, which was used in the wetting studies.[39] The experimentally determined values of the Hamaker constant are found to be in a good agreement with theoretical predictions. In particular, a very good agreement is observed for SPEEK when $\boldsymbol{A}_{\mathbf{H_L}}$ is

compared to the experimental Hamaker constant calculated using eq 7 and 5, i.e. for the scenario where the dragging force is divided between two fiber contacts. By contrast, for PVA we observe a very good agreement for the case of a single contact model, i.e. $\langle F_{\mathrm{TOTAL}} \rangle \approx \{F_{\mathrm{adh}}\}$. Although these values should be taken as an order of magnitude approximation, we can hypothesize that the structure of the network may play a role in determining the probability of pulling configurations. From Figure 1 one can see that fibers in the SPEEK electrospun matt are more regularly aligned compared to PVA, where many fibers are being curled and entangled into bundles containing more than two fibers. Thus, a more grid-like configuration of SPEEK fiber matts may favor configurations that involve two-fiber contacts.

## CONCLUSIONS

We present a novel technique for measuring the adhesion between individual nano-fibers. Currently, there are technical challenges associated with isolating and handling individual nano-fibers for measuring the adhesion between them in cross and parallel configurations. In this study, we used an AFM cantilever tip to drag fibers out of a network and measure the pull-off force. This technique has the unique advantage of working directly with fibrous networks which inherently have a distribution of fiber diameters and orientations. We consider the most frequent value from the distribution of detachment forces to represent the pull-off force corresponding to the event where a single fiber contact is probed. The experimental results are in good agreement with theoretical adhesion for the nanofibers (electrospun SPEEK, electrospun PVA) which interact through van der Waals forces. The pull-off forces between fibers evaluated from the presented technique can provide data for network models of fibrous systems and assist with advanced biomaterial design.

## TABLES.

**Table 1. The exponentially averaged peak height values from a set of force-distance curves measured for SPEEK samples referenced A-E for increasing network density. Total number of peak events is 280.**

| Sample Reference | Peak Height (μN) |
|---|---|
| A | 6.8 |
| B | 6.9 |
| C | 11 |
| D | 7.3 |
| E | 10 |

**Table 2. The experimental and theoretical values of the Hamaker constant ($A_H$) for SPEEK and PVA. The theoretical values are calculated using the surface energy approach ($A_{H_{SE}}$), and the full Lifshitz' theory calculation using the integrated form of the equation for the free energy of interaction developed by Parsegian and Ninham ($A_{H_L}$) (see text for details of the calculation). The experimental values are calculated using eq 7 and (i) the average experimental values of pull-off forces ($A_{H_{exp}}$), (ii) the average experimental values of pull-off forces adjusted using a correction factor from eq 5 that corresponds to the scenario where the dragging force is divided between two fiber contacts ($A_{H_{exp^\circ}}$).**

| | $F_{pull-off}$ [$\mu N$] | $A_{H_{SE}}$ [J $\cdot 10^{-20}$] | $A_{H_L}$ [J $\cdot 10^{-20}$] | $A_{H_{exp}}$ [J $\cdot 10^{-20}$] | $A_{H_{exp^\circ}}$ [J $\cdot 10^{-20}$] | $L$ [nm] |
|---|---|---|---|---|---|---|
| **SPEEK** | 8.4 | 5.8 | 12.9 | 16.07 | 12.6 | 331 |
| **PVA** | 6.1 | 10.5 | 10.5 | 9.4 | 7.4 | 362 |

FIGURES

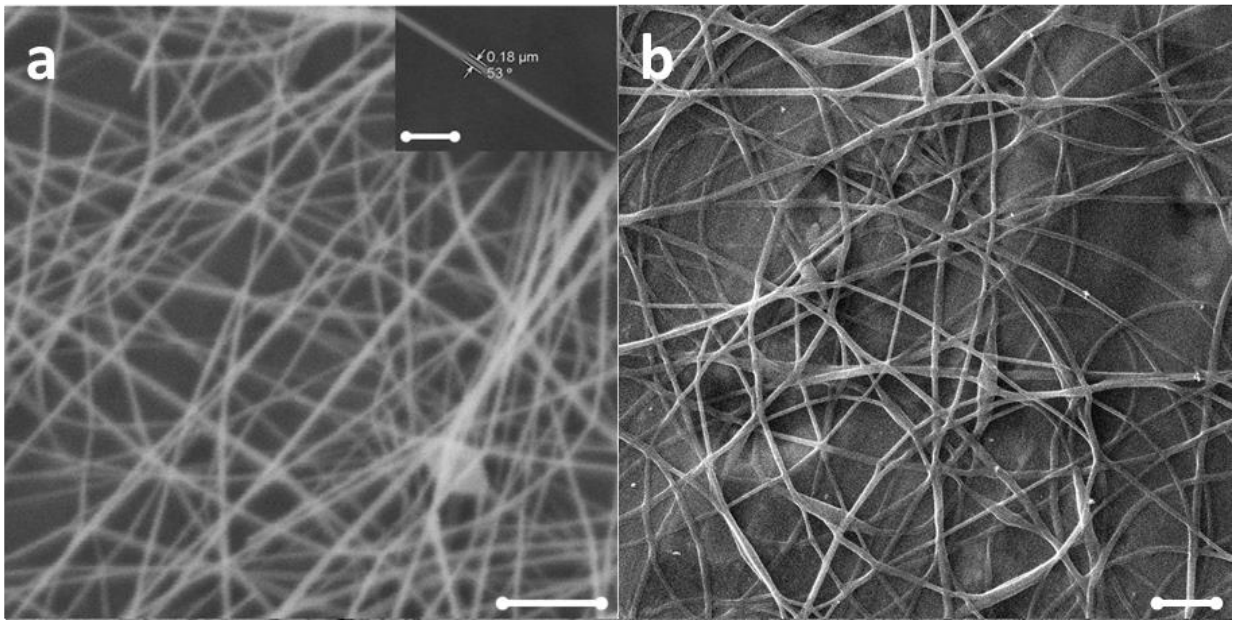


**Figure 1. Microscopy images of nano-fibrous networks. (a) SEM micrograph of electrospun SPEEK nanofiber network (scale bar is 1 µm). The inset shows a single SPEEK fiber with the corresponding diameter measurement (scale bar is 1 µm) (b) SEM micrograph of electrospun PVA nanofiber network (scale bar is 2 µm).**

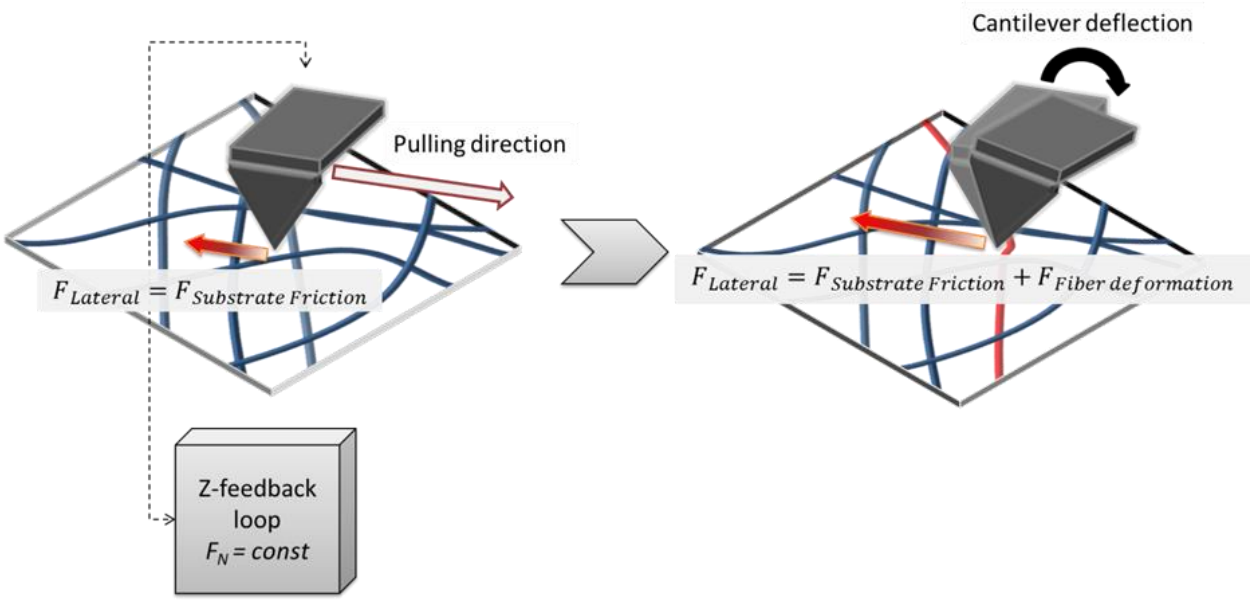


**Figure 2. The AFM tip is engaged with the substrate at a constant normal force and moved in a lateral pulling direction. The initial lateral force is due to friction between the cantilever tip and substrate. When the tip engages with a fiber the lateral force increases due to fiber deformation until a detachment event occurs at a fiber-fiber contact in the network.**

a b

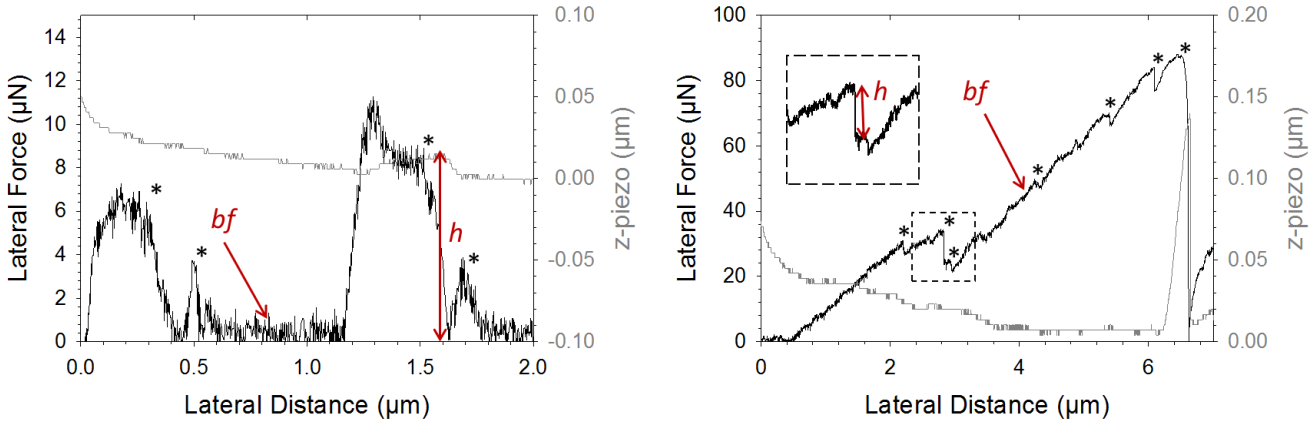


**Figure 3. Typical lateral force-distance curves for SPEEK samples with (a) constant and (b) increasing baseline force (bf). (*) denotes the peak events identified during data processing. The peak height (h), calculated as the distance between the maximum and subsequent minimum of the peak is labelled. The z-piezo position of the cantilever holder relative to the substrate is plotted on the right-hand y-axis.**

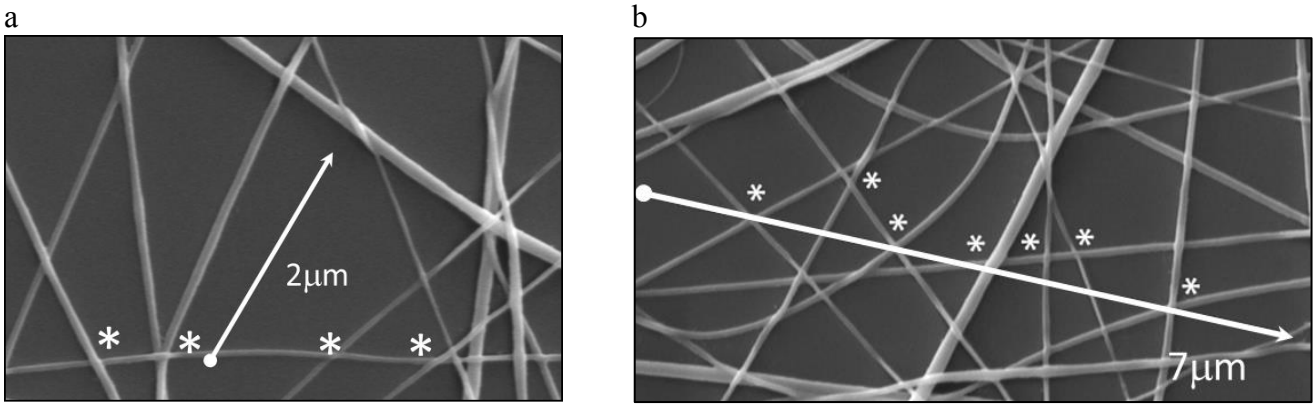


**Figure 4.**

**(a) and (b) show SEM images superimposed with proposed cantilever traces corresponding to the lateral distances measured for respective SPEEK samples in Figure 3 (a) and (b).**

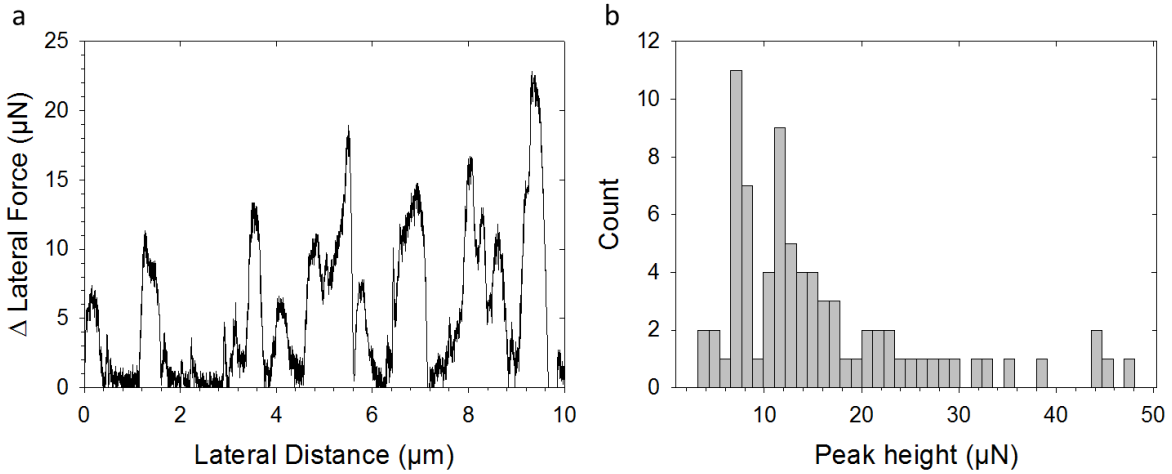


**Figure 5. Analysis of example force distance curve for SPEEK sample showing (a) representative force-distance curve and (b) histogram of peak heights obtained from an entire series of curves.**

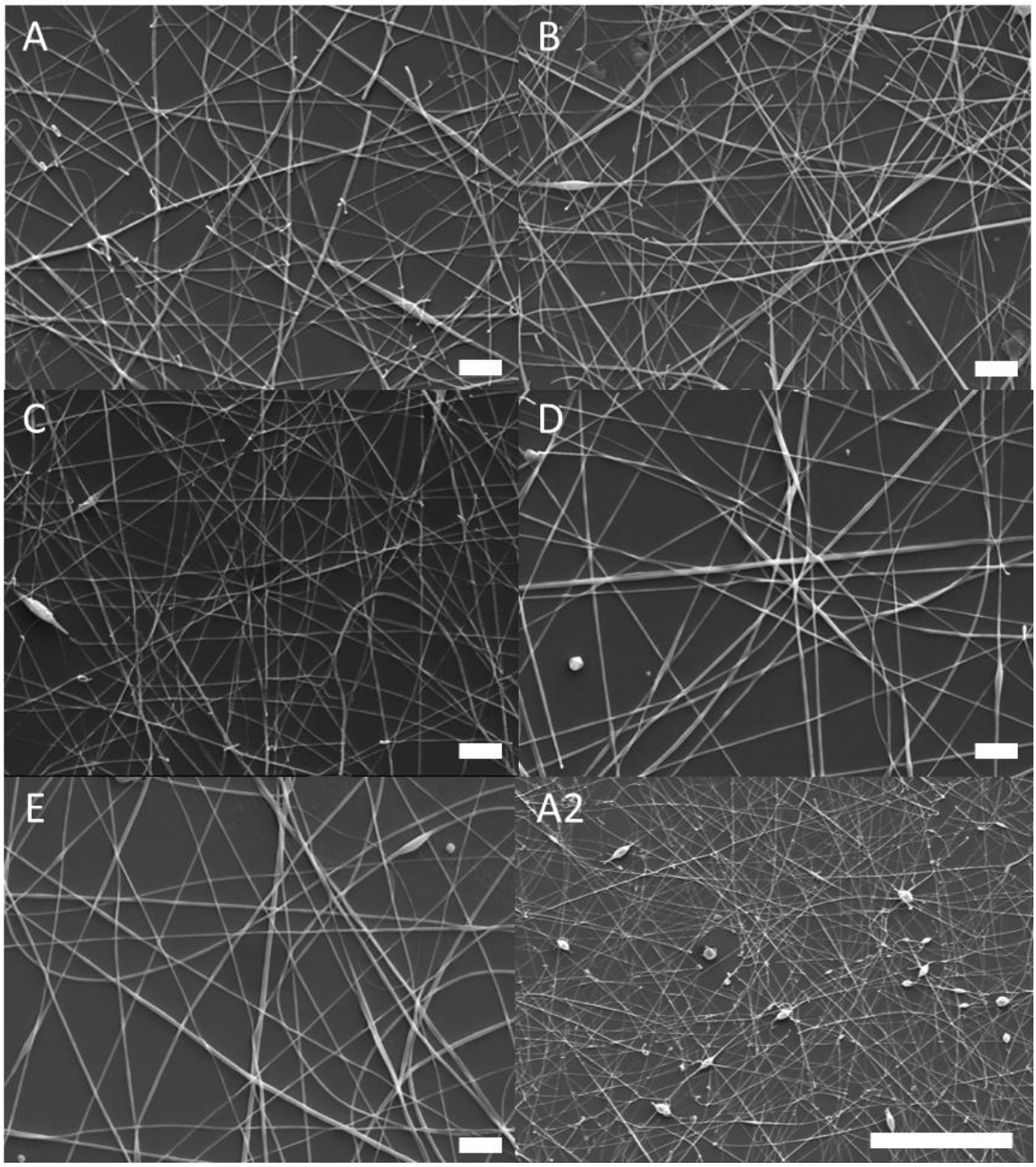


**Figure 6. SEM micrographs at 10 000 x magnification of electrospun SPEEK nanofiber networks with different electrospinning times labelled A through to E (scale bar is 1 µm). A2 is an SEM micrograph of substrate A at 2000 x magnification showing the breakages of fibers around the globular-like structures.**

a

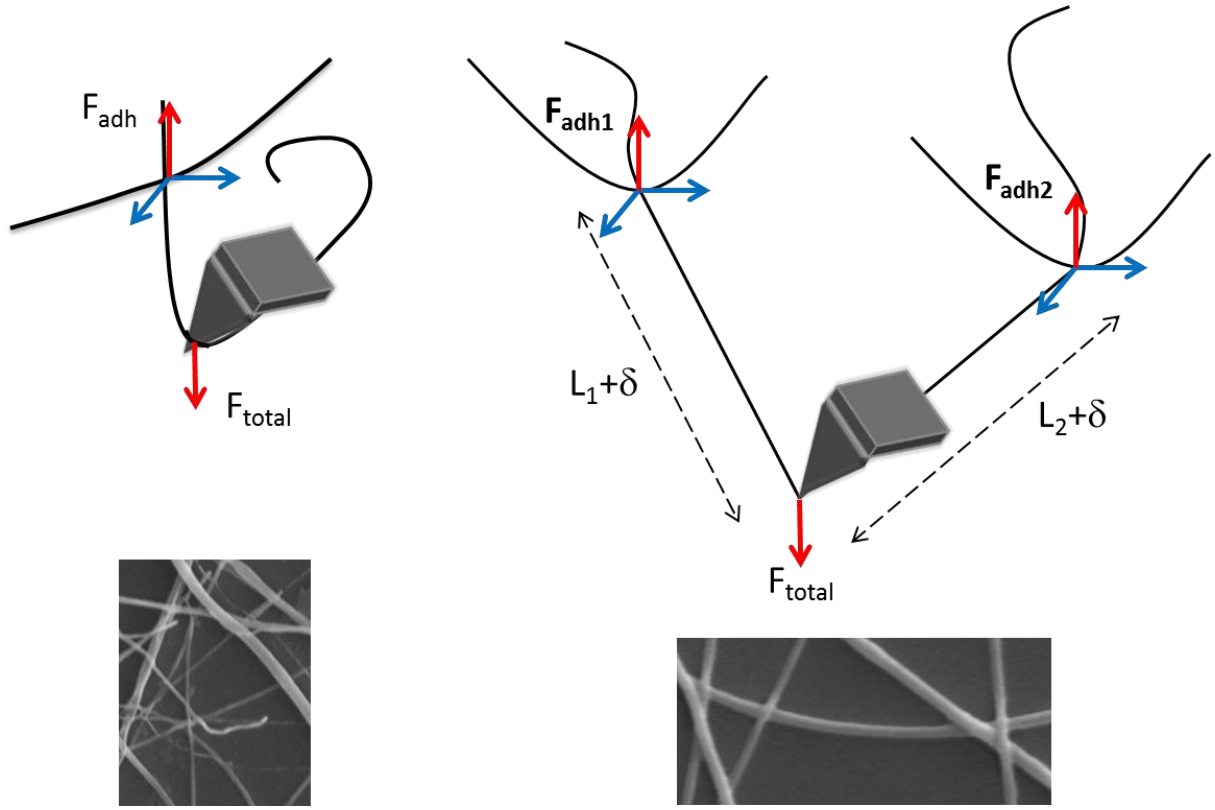


b

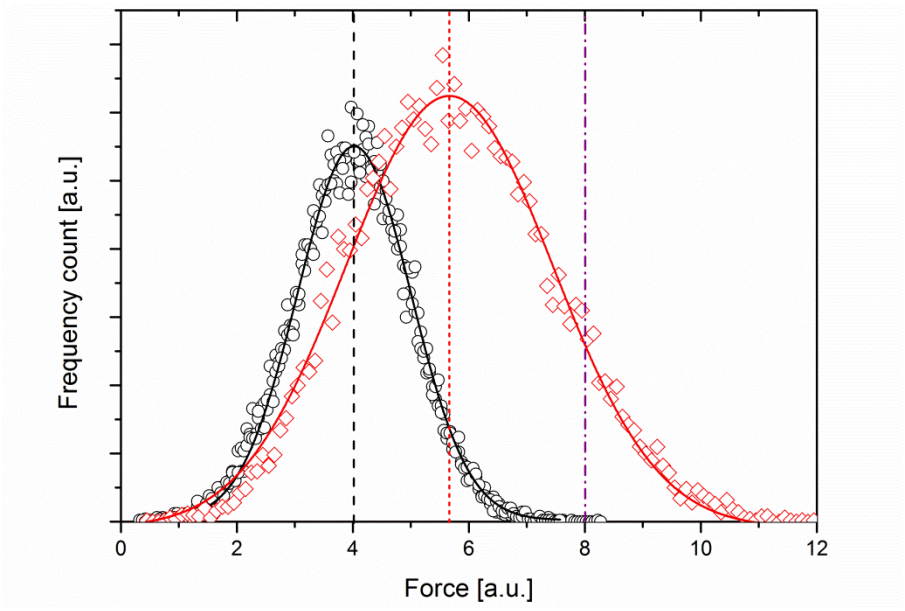


**Figure 7. (a) Illustrations of two possible scenarios for pulling a fiber and probing either 1 or 2 contact points. The insets show the SEM images of the SPEEK networks that may illustrate the microscopic representation of such scenarios. (b) A theoretical model of a pull-off experiment based on 10 000 junctions with normally distributed inter-fiber adhesive energies. Open circles represent the frequency distribution of pull-off forces for Scenario 1. Open diamonds represent the corresponding distribution of pull-off forces for Scenario 2, calculated based on eq 2 and a uniform distribution of the parameter $l = L_1/L_2$, which corresponds to the random position of the AFM tip with respect to the contact points. Solid lines are best fits using Gaussian function. Dash lines mark the most frequent value of pull-off force for each scenario. The dash-dot line marks the force value for the case of a symmetric pull, i.e., $l = 1$.**

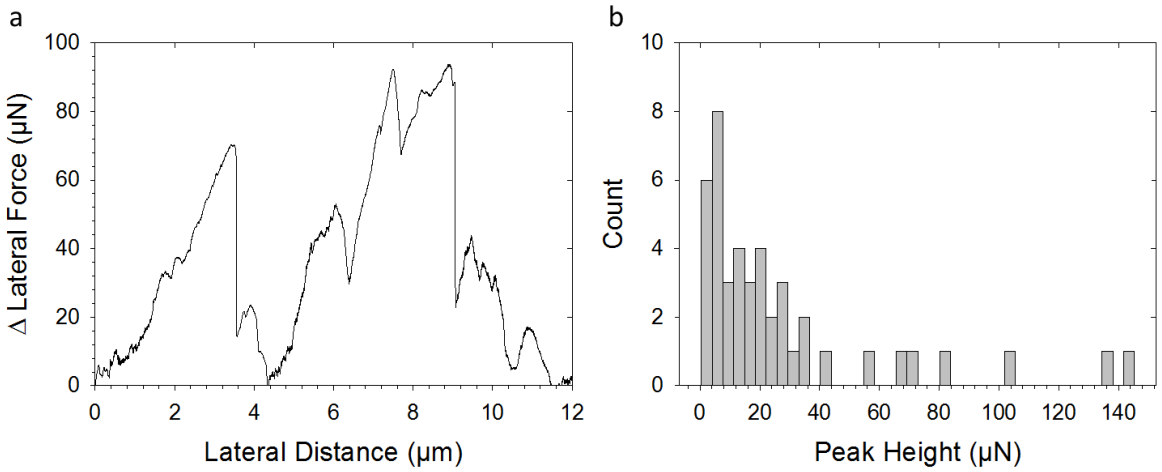


**Figure 8. (a) Representative force-distance curve for PVA and (b) histogram of peak height values for the entire set of curves.**

## AUTHOR INFORMATION


### Corresponding Author

* E-mail: Gleb.Yakubov@uq.edu.au.


### Notes

The authors declare no competing financial interest.

## ACKNOWLEDGMENT

Dr. Xiaoen Wang is acknowledged for his help in preparing the SPEEK fibers. Dr Mauricio R. Bonilla is acknowledged for many helpful discussions of pull-off mechanisms. This work was performed in part at the Queensland node of the Australian National Fabrication Facility (ANNF-Q), a company established under the National Collaborative Research Infrastructure Strategy to provide nano- and microfabrication facilities for Australia's researchers. This work was supported by the Australian Research Council (ARC) through the ARC Discovery Project (DP150104147), the ARC Centre of Excellence in Plant Cell Walls (CE110001007), The University of Queensland (UQ Advantage Scholarship), and the Australian Postgraduate Award (APA Scholarship).

## REFERENCES


(1) Gutsmann, T.; Fantner, G. E.; Kindt, J. H.; Venturoni, M.; Danielsen, S.; Hansma, P. K. Force spectroscopy of collagen fibers to investigate their mechanical properties and structural organization. *Biophysical Journal* **2004,** *86* (5), 3186-3193.

(2) Miletzky, A.; Fischer, W. J.; Czibula, C.; Teichert, C.; Bauer, W.; Schennach, R. How xylan effects the breaking load of individual fiber-fiber joints and the single fiber tensile strength. *Cellulose* **2015,** *22* (1), 849-859.

(3) Yan, Y. a. L., K. Evaluation of inter-fiber bonding in wood pulp fibers by chemical force microscopy. *Journal of Materials Science Research* **2013,** *2* (1), 23-33.

(4) Chen, X.; Wu, G.; Feng, Z.; Dong, Y.; Zhou, W.; Li, B.; Bai, S.; Zhao, Y. Advanced biomaterials and their potential applications in the treatment of periodontal disease. *Critical Reviews in Biotechnology* **2015**, 1-16.

(5) Schaub, N. J.; Gilbert, R. J. Controlled release of 6-aminonicotinamide from aligned, electrospun fibers alters astrocyte metabolism and dorsal root ganglia neurite outgrowth. *Journal of Neural Engineering* **2011,** *8* (4).

(6) Hsu, F. Y.; Weng, R. C.; Lin, H. M.; Lin, Y. H.; Lu, M. R.; Yu, J. L.; Hsu, H. W. A biomimetic extracellular matrix composed of mesoporous bioactive glass as a bone graft material. *Microporous and Mesoporous Materials* **2015,** *212*, 56-65.

(7) Pelipenko, J.; Kocbek, P.; Kristl, J. Critical attributes of nanofibers: Preparation, drug loading, and tissue regeneration. *International Journal of Pharmaceutics* **2015,** *484* (1-2), 57-74.

(8) Chanliaud, E.; Burrows, K. M.; Jeronimidis, G.; Gidley, M. J. Mechanical properties of primary plant cell wall analogues. *Planta* **2002,** *215* (6), 989-996.

(9) Huang, R.; Li, W. Z.; Lv, X. X.; Lei, Z. J.; Bian, Y. Q.; Deng, H. B.; Wang, H. J.; Li, J. Q.; Li, X. Y. Biomimetic LBL structured nanofibrous matrices assembled by chitosan/collagen for promoting wound healing. *Biomaterials* **2015,** *53*, 58-75.

(10) Janmey, P. A.; Euteneuer, U.; Traub, P.; Schliwa, M. Viscoelastic properties of vimentin compared with other filamentous biopolymer networks. *Journal of Cell Biology* **1991,** *113* (1), 155-160.

(11) Leterrier, J. F.; Kas, J.; Hartwig, J.; Vegners, R.; Janmey, P. A. Mechanical effects of neurofilament cross-bridges - Modulation by phosphorylation, lipids, and interactions with F-actin. *Journal of Biological Chemistry* **1996,** *271* (26), 15687-15694.

(12) Lopez-Sanchez, P.; Rincon, M.; Wang, D.; Brulhart, S.; Stokes, J. R.; Gidley, M. J. Micromechanics and poroelasticity of hydrated cellulose networks. *Biomacromolecules* **2014,** *15* (6), 2274-2284.

(13) Ma, L. L.; Xu, J. Y.; Coulombe, P. A.; Wirtz, D. Keratin filament suspensions show unique micromechanical properties. *Journal of Biological Chemistry* **1999,** *274* (27), 19145-19151.

(14) Poquillon, D.; Viguier, B.; Andrieu, E. Experimental data about mechanical behaviour during compression tests for various matted fibres. *Journal of Materials Science* **2005,** *40* (22), 5963-5970.

(15) Tseng, Y.; An, K. M.; Esue, O.; Wirtz, D. The bimodal role of filamin in controlling the architecture and mechanics of F-actin networks. *Journal of Biological Chemistry* **2004,** *279* (3), 1819-1826.

(16) Whitney, S. E. C.; Gothard, M. G. E.; Mitchell, J. T.; Gidley, M. J. Roles of cellulose and xyloglucan in determining the mechanical properties of primary plant cell walls. *Plant Physiology* **1999,** *121* (2), 657-663.

(17) Zhou, L.; He, H.; Jiang, C.; He, S. Preparation and characterization of poly(glycerol sebacate)/cellulose nanocrystals elastomeric composites. *Journal of Applied Polymer Science* **2015,** *132* (27).

(18) Zou, Y.; Zhang, Y. H. An experimental and theoretical study on the anisotropy of elastin network. *Annals of Biomedical Engineering* **2009,** *37* (8), 1572-1583.

(19) Komori, T.; Itoh, M. A new approach to the theory of the compression of fiber assemblies. *Textile Research Journal* **1991,** *61* (7), 420-428.

(20) Narter, M. A.; Batra, S. K.; Buchanan, D. R. Micromechanics of three-dimensional fibrewebs: constitutive equations. *Proceedings of the Royal Society a-Mathematical Physical and Engineering Sciences* **1999,** *455* (1989), 3543-3563.

(21) Wang, C. W.; Berhan, L.; Sastry, A. M. Structure, mechanics and failure of stochastic fibrous networks: Part I - Microscale considerations. *Journal of Engineering Materials and Technology-Transactions of the Asme* **2000,** *122* (4), 450-459.

(22) Wu, X. F.; Dzenis, Y. A. Elasticity of planar fiber networks. *Journal of Applied Physics* **2005,** *98* (9).

(23) Chatterjee, A. P. A model for the elastic moduli of three-dimensional fiber networks and nanocomposites. *Journal of Applied Physics* **2006,** *100* (5).

(24) Shi, Q.; Wan, K.-T.; Wong, S.-C.; Chen, P.; Blackledge, T. A. Do electrospun polymer fibers stick? *Langmuir* **2010,** *26* (17), 14188-14193.

(25) Shi, Q.; Wong, S.-C.; Ye, W.; Hou, J.; Zhao, J.; Yin, J. Mechanism of adhesion between polymer fibers at nanoscale contacts. *Langmuir* **2012,** *28* (10), 4663-4671.

(26) Wang, X.; Najem, J. F.; Wong, S.-C.; Wan, K.-t. A nano-cheese-cutter to directly measure interfacial adhesion of freestanding nano-fibers. *Journal of Applied Physics* **2012,** *111* (2).

(27) Stachewicz, U.; Hang, F.; Barber, A. H. Adhesion anisotropy between contacting electrospun fibers. *Langmuir* **2014,** *30* (23), 6819-6825.

(28) Xing, M.; Zhong, W.; Xu, X. L.; Thomson, D. Adhesion force studies of nanofibers and nanoparticles. *Langmuir* **2010,** *26* (14), 11809-11814.

(29) Huang, R. Y. M.; Shao, P. H.; Burns, C. M.; Feng, X. Sulfonation of poly(ether ether ketone)(PEEK): Kinetic study and characterization. *Journal of Applied Polymer Science* **2001,** *82* (11), 2651-2660.

(30) Feiler, A. A.; Bergstrom, L.; Rutland, M. W. Superlubricity using repulsive van der Waals forces. *Langmuir* **2008,** *24* (6), 2274-2276.

(31) Dzyaloshinskii, I. E.; Lifshitz, E. M.; Pitaevskii, L. P. The general theory of van der Waals forces. *Advances in Physics* **1961,** *10* (38), 165-209.

(32) Green, C. P.; Lioe, H.; Cleveland, J. P.; Proksch, R.; Mulvaney, P.; Sader, J. E. Normal and torsional spring constants of atomic force microscope cantilevers. *Review of Scientific Instruments* **2004,** *75* (6), 1988-1996.

(33) Wagner, K.; Cheng, P.; Vezenov, D. Noncontact method for calibration of lateral forces in scanning force microscopy. *Langmuir* **2011,** *27* (8), 4635-4644.

(34) Munz, M. Force calibration in lateral force microscopy: a review of the experimental methods. *Journal of Physics D-Applied Physics* **2010,** *43* (6).

(35) Jarzynski, C. Nonequilibrium equality for free energy differences. *Physical Review Letters* **1997,** *78* (14), 2690-2693.

(36) Jarzynski, C. Equilibrium free-energy differences from nonequilibrium measurements: A master-equation approach. *Physical Review E* **1997,** *56* (5), 5018-5035.

(37) Israelachvili, J. N. *Intermolecular and Surface Forces, 3rd Edition* 2011. p 1-674.

(38) Vial, J.; Carre, A. Calculation of Hamaker constant and surface-energy of polymers by a simple-group contribution method. *International Journal of Adhesion and Adhesives* **1991,** *11* (3), 140-143.

(39) Kanakasabai, P.; Vijay, P.; Deshpande, A. P.; Varughese, S. Crosslinked poly(vinyl alcohol)/sulfonated poly(ether ether ketone) blend membranes for fuel cell applications-Surface energy characteristics and proton conductivity. *Journal of Power Sources* **2011,** *196* (3), 946-955.

(40) Parsegian, V. A.; Ninham, B. W. van der Waals forces in many-layered structures: Generalizations of Lifshitz result for two semi-infinite media. *Journal of Theoretical Biology* **1973,** *38* (1), 101-109.

(41) Hough, D. B.; White, L. R. The calculation of Hamaker constants from Lifshitz theory with applications to wetting phenomena. *Advances in Colloid and Interface Science* **1980,** *14* (1), 3-41.

(42) Cavalier, K.; Larche, F. Hamaker constants of solids in di-octylphthalate. *Colloids and Surfaces a-Physicochemical and Engineering Aspects* **2006,** *276* (1-3), 143-145.

(43) Koziara, B. T.; Nijmeijer, K.; Benes, N. E. Optical anisotropy, molecular orientations, and internal stresses in thin sulfonated poly(ether ether ketone) films. *Journal of Materials Science* **2015,** *50* (8), 3031-3040.

(44) Mahendia, S.; Tomar, A. K.; Chahal, R. P.; Goyal, P.; Kumar, S. Optical and structural properties of poly(vinyl alcohol) films embedded with citrate-stabilized gold nanoparticles. *Journal of Physics D-Applied Physics* **2011,** *44* (20).

(45) Song, J. M.; Shin, J.; Sohn, J. Y.; Nho, Y. C. Preparation and characterization of SPEEK membranes crosslinked by electron beam irradiation. *Macromolecular Research* **2011,** *19* (10), 1082-1089.

(46) Changkhamchom, S.; Sirivat, A. Synthesis and properties of sulfonated poly(ether ketone ether sulfone) (S-PEKES) via bisphenol S: effect of sulfonation. *Polymer Bulletin* **2010,** *65* (3), 265-281.

(47) El-Sayed, S.; Mahmoud, K. H.; Fatah, A. A.; Hassen, A. DSC, TGA and dielectric properties of carboxymethyl cellulose/polyvinyl alcohol blends. *Physica B-Condensed Matter* **2011,** *406* (21), 4068-4076.

Table of Contents artwork